Design of elastomer coatings for concrete impact damage mitigation

C. Fallon[a], G.J. McShane[a,*]

[a]*Department of Engineering, University of Cambridge, Trumpington Street, Cambridge CB2 1PZ, UK*

Abstract

Practical, cost-effective strategies are of interest for the protection of vulnerable infrastructure against dynamic load events such as blast and fragment impact. Recent research has established that spray-on elastomer coatings can provide a significant impact mitigating effect when applied to concrete structural elements [1]. However, to date, no practical design guidelines exist to support efficient implementation of this retrofit solution. In this work, an analytical model is proposed for the impact indentation of an elastomer-coated concrete structural element. Design maps are produced, predicting the critical projectile impact velocities for elastomer failure and concrete failure, taking the coating thickness and elastomer modulus as the key design variables. The analytical predictions provide a close match to experimental and finite element analysis (FEA) results [1, 2]. Spanning a realistic range of elastomer moduli, representative of typical spray application polymers, a regime change is predicted that depends only on the elastomer modulus, E_e. For $E_e < 50\,\mathrm{MPa}$, elastomer failure is predicted to occur first. In this regime, there is a much higher sensitivity to E_e compared with the elastomer thickness, h_e. For $E_e > 50\,\mathrm{MPa}$, the concrete is predicted to fail first and in this regime, the critical velocities are most sensitive to h_e compared with E_e.
Keywords: impact, concrete, elastomer, coating, design, analytical model

*Corresponding author
Email addresses: cf335@cam.ac.uk (C. Fallon), gjm31@cam.ac.uk (G.J. McShane)

1. Introduction

With growing levels of malevolent attack at the forefront of political and industrial agendas, new strategies are needed to protect civilian infrastructure and its inhabitants from blast and fragment impact events. In recent years, there has been increasing interest in the development of protective strategies that combine practicality and cost-effectiveness in the design of both new-build projects, and in the retrofit of older buildings, against the evolving threat of improvised explosive devices (including blast and fragment impact events). Although protective performance of the chosen solution is key, careful consideration must be given to reducing cost, ease of installation, low life-time maintenance requirements and preserving aesthetics.

One retrofit solution that has been gaining attention is the use of a spray-application elastomer coating, applied to existing urban infrastructure. Their spray application gives these coatings a distinct advantage over other candidate retrofits (e.g. fibre-reinforced polymer composites) which are often more expensive and difficult to install [3, 4]. Early experimental blast trials examined such coatings applied to masonry wall structures which yielded encouraging results [3, 5] but despite the potential demonstrated, only a very limited number of studies have extended consideration to the retrofit of concrete and reinforced concrete (RC) structures. Concrete appears the ideal candidate to benefit from this type of retrofit, representing the most significant proportion of the ageing, vulnerable infrastructure in today's built environment. Recent work has focused on the blast response of elastomer-coated concrete [6–8] and has suggested that the coating is only effective in high intensity blast regimes, when the concrete has already been severely damaged.

In this investigation, we focus on the protective performance of a polymer coating applied to concrete, and subjected to projectile impact. A recent experimental study has explored the impact-mitigating capabilities of this retrofit solution [1]. Relatively thin elastomer coatings were applied to 100 mm side length concrete cubes and were impacted with 0.1 kg circular cylindrical (*i.e.* blunt) steel projectiles. A significant protective benefit was observed across the range of impact velocities tested, $45 - 150\,\mathrm{m\,s^{-1}}$. This prompted the development of a numerical model to simulate the dynamic impact tests with the objective of interrogating the mechanism by which the elastomer achieves its protective effect. Focusing on damage initiation in the concrete, two damage mechanisms were identified [2]. Mechanism 1, characterised by severe concrete damage, initiating early under the indenter corner, and Mechanism 2, characterised by more diffuse, sub-surface concrete damage developing over longer timescales. At high impact velocities, the damage pattern develops to form a cone of compressive damage under the indenter over longer timescales. It was established that the addition of an elastomer coating serves two effects: (i) the impact speed at which damage first occurs is increased and (ii) the damage initiation mechanism shifts from Mechanism 1 to Mechanism 2. Upon detailed interrogation of simplified FE models, it was concluded that the elastomer achieves its protective effect via two mechanisms — a *temporal effect* (a reduction in the magnitude of the peak acceleration and an increase in the contact duration between the projectile and target), and a *spatial effect* (a more uniform contact pressure distribution is achieved, removing stress concentrations under the indenter corner).

The objective of the present study is to build upon the aforementioned work [1, 2] to develop guidelines for effective coating design for concrete impact damage mitigation. As in [1, 2], we focus on the mechanisms of damage initiation and the role of the coating for the early timescale response to impact. As discussed in [2], this damage initiation response appears to play a key role in the way damage subsequently develops at longer timescales. There is also more confidence in the predictive accuracy of the FE model before the damage becomes extensive. The experimental results and numerical model predictions from [1, 2] are first compared and used to identify the regimes of concrete failure/no failure for a range of realistic coating thicknesses and projectile impact velocities. Practical fragment impact loads may span a wide range of projectile masses, geometries and impact speeds. Each of these variables may alter the key damage and protection mechanisms. We focus in this investigation on one case, the impact loading scenario addressed in [1, 2]: normal impact with a flat-faced (*i.e.* blunt) cylindrical projectile. The projectile has a mass, 0.1 kg and impact velocities up to $150\,\mathrm{m\,s^{-1}}$ are considered. From a design perspective, delaying the failure of the concrete substrate is of critical importance. An analytical model is developed, capable of predicting the critical projectile impact velocities for failure for an elastomer-coated concrete target subjected to blunt projectile impact. Practical design maps are derived using the proposed analytical models, taking the key variables as the coating thickness and elastomer modulus. Finally, the analytical model is validated by comparison with experimental results and FEA predictions obtained in [1, 2].

2. Modelling the impact response of elastomer-coated concrete

A series of quasi-static indentation and dynamic, gas gun tests were reported in [1] using a 0.1 kg, 28.5 mm diameter circular cylindrical (i.e. blunt) steel indenter. Impact testing was performed on 100 mm side length concrete cubes, coated with a 5 mm thick elastomer layer positioned on their impacted face. The elastomer layer was not bonded to the concrete but was in frictional contact only. It is shown in [1] that the elastomer contributes a significant protective benefit over the range of impact velocities tested, $45 - 150\,\mathrm{m\,s^{-1}}$. The coating fails by a ductile plugging mechanism when impacted at speeds in excess of *c.* $125\,\mathrm{m\,s^{-1}}$.

A finite element model is developed in Abaqus/Explicit and is validated against both quasi-static and dynamic experimental tests [1]. Focusing on the early time steps, the model is used to interrogate the elastomer's influence on the damage initiation regimes in the concrete [2]. Further, the mechanisms by which the coating contributes its mitigating effect are assessed. The axisymmetric numerical model developed in [1, 2] for the dynamic impact tests is reproduced in Fig. 1.

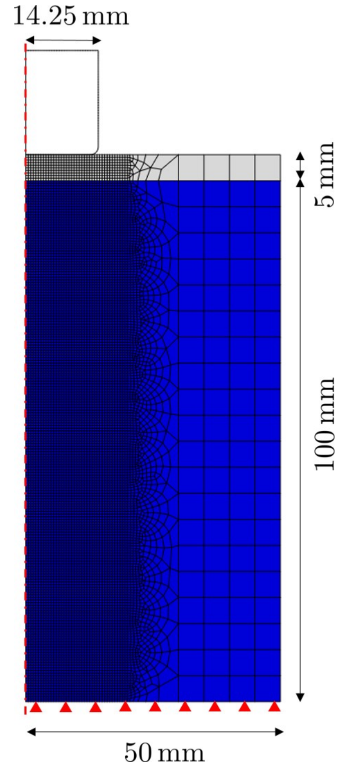

Figure 1: Axisymmetric model developed in [1, 2] used to interrogate the impact indentation response of elastomer-coated concrete cubes.

The details of this model are presented in [1, 2] but are summarised here. The Concrete Damaged Plasticity (CDP) model is employed for the concrete constitutive model definition. A compressive strength of 47 MPa, Young's Modulus, 28.3 GPa and density $2550\,\mathrm{kg\,m^{-3}}$ are chosen. The CDP model assumes concrete to be a homogeneous continuum, modelling pressure-dependent plasticity and damaged elasticity with damage prescribed in terms of tensile, d_t and compressive, d_c damage parameters. These damage parameters can take values between 0 (undamaged material) and 1 (fully damaged material).

To model the elastomer coating, a series of material characterisation tests are performed on a sample of a commercially available, polyurea/polyurethane hybrid [7]. A hyperelastic constitutive relationship is selected, fitted to the uniaxial tensile response up to a nominal strain, $\epsilon = 1$, using data measured at a nominal strain rate, $10^{-3}\,\mathrm{s^{-1}}$. The Yeoh strain energy potential is chosen as it is deemed to provide the best fit to experimental measurements. Viscoelasticity is incorporated via a Prony series for similar materials, obtained from the literature (Table 3.4 in [9]). The polymer is assumed to be nearly incompressible, with a Poisson's ratio, $\nu = 0.475$ (note that a finite bulk modulus is required, for numerical purposes). The polymer has a density of $1.1\,\mathrm{Mg\,m^{-3}}$. The model has been shown to predict well the tensile, compressive and indentation response of the polymer at a range of strain rates ($10^{-3} - 10^{2}\,\mathrm{s^{-1}}$) [1, 7]. In [1], to assess the model's validity at higher strain rates, numerical predictions for the projectile velocity-time histories are compared to those measured using high speed photography during the impact experiments on coated concrete (for projectile impact velocities up to $\sim 100\,\mathrm{m\,s^{-1}}$). Excellent agreement was observed for the loading response of the curve, up to the point of maximum projectile penetration.

The projectile is modelled as a rigid part with a small corner radius, 1.5 mm, to capture accurately the behaviour of a flat nosed projectile, while avoiding the stress singularity associated with a truly sharp corner. The size of the corner radius, and the corresponding mesh size in the concrete target, was chosen based on a detailed sensitivity study [1].

The concrete and elastomer are meshed using 4-node, axisymmetric elements with a fine, 0.5 mm element size directly under the indenter, transitioning to a coarser 5 mm mesh, well away from the impact site. Based on a good match to quasi-static indentation experiments, frictionless contact is assumed between concrete/steel interfaces whereas frictional contact (with a coefficient of friction, $\mu = 0.8$) is implemented between elastomer/concrete interfaces [1] enforced by prescribing the tangential behaviour using a penalty contact formulation.

3. Identification of impact response regime boundaries

These FE models are used to vary the projectile velocity, V_0 and the polymer thickness, h_e, in order to populate a map, plotting the combination of these variables that give rise to concrete damage. This map is illustrated in Fig 2a. The compressive damage parameter, d_c is used as the concrete damage metric. When a specified number of concrete elements (extending to a depth of approximately 5 mm) have reached $d_c > 0.9$ during the loading portion of the indentation response, the concrete is deemed to be damaged. As observed in [1, 2], compressive damage dominates the response, initiating under the indenter corner at very early timesteps of the order of microseconds.

Also plotted on Fig. 2a are the results from the experimental gas gun tests presented in

[1]. In the experimental tests, concrete damage is determined on the basis of post-impact visual inspection, where a block exhibiting visible cracking or complete fragmentation is deemed damaged.

Comparing the FE predictions and experimental observations in Fig. 2a, the results agree well, particularly for $V_0 < 75\,\mathrm{m\,s^{-1}}$ and $V_0 > 120\,\mathrm{m\,s^{-1}}$. However the FE model appears to underpredict the impact damage resistance, predicting damage for a 6 mm elastomer-coated block impacted at $V_0 = 100\,\mathrm{m\,s^{-1}}$, when there was no visible damage observed in the corresponding experiment. There are a number of potential contributory factors to this discrepancy. The concrete constitutive model does not allow for strain rate dependence, which could influence the concrete strength at higher projectile impact speeds. Furthermore, the elastomer constitutive model does not include a failure criterion. This would provide an additional dissipative mechanism, absent from the current analysis. Another is the friction between the coating and the concrete, which we proceed to address in further detail.

As described in [1], frictional contact is chosen, with a friction coefficient of $\mu = 0.8$ at the concrete/elastomer interface, based on best fit with quasi-static experimental results. However, it is indicated in [1] that frictionless contact at this interface agreed better with dynamic tests, providing a closer estimate of the projectile rebound velocities measured using high speed photography. For that study, the influence of these frictional effects were difficult to determine given other obscuring factors such as severe concrete damage and lack of elastomer hysteresis in the numerical model. Here, this question is revisited. Figure 2b plots the comparison between the experimental results and the FE predictions, assuming frictionless contact for the tangential behaviour at the elastomer/concrete interface. This serves to reduce predicted concrete damage for a given impact velocity, bringing the FE predictions more into line with the experimental observations.

This suggests that the frictional contact conditions may, indeed, depend on the strain rate. Considering that the elastomer is not bonded to the concrete substrate, it is reasonable to assume that the frictional conditions experienced at this interface may be influenced by the elastomeric response, which is itself time-dependent. Alternatively, premature concrete failure during the dynamic FE simulations assuming frictional contact may be due to the sensitivity of the concrete failure model to the induced surface tractions at the con-

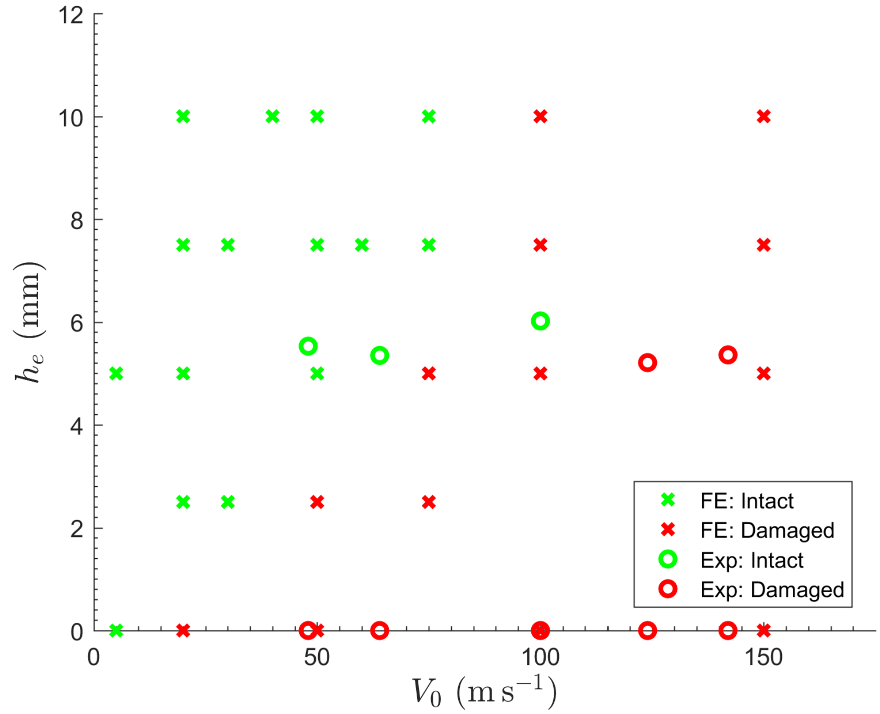

(a) Friction with coefficient, $\mu = 0.8$

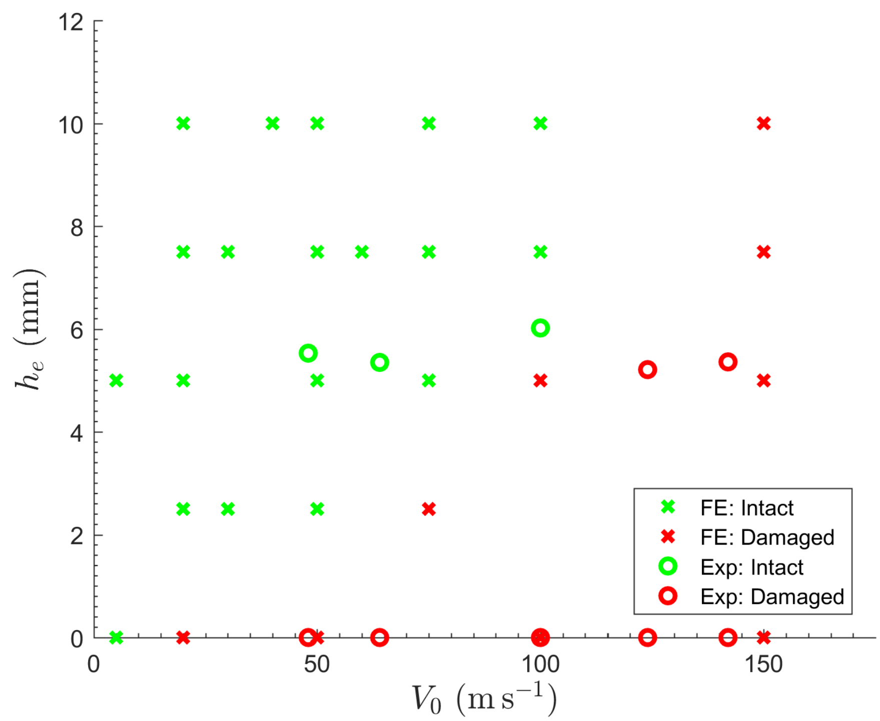

(b) Frictionless

Figure 2: Comparison between FE predictions and experimental observations. Two variations of the FE model are considered: (a) Frictional contact at the concrete/elastomer interface with a coefficient, $\mu = 0.8$ and (b) Frictionless contact at the concrete/elastomer interface. Legend: $\times$ represents FE predictions and $\circ$ represents experimental observations; green indicates intact concrete and red indicates damaged concrete.

crete/elastomer interface. The model may lose fidelity under the complex stress state at this interface, resulting in a more severe damage prediction.

In the following sections, FE predictions are presented for both contact conditions: (i) frictional contact at the elastomer/concrete interface (with a coefficient of friction, $\mu = 0.8$) and (ii) frictionless contact at that interface.

4. Analytical modelling

The aim now is to derive an analytical model capable of predicting the onset of failure for elastomer-coated concrete targets. The motivation is derived from the findings in [2], which identify the key mechanisms responsible for the elastomer's protective effect.

Normal impact from a rigid projectile of radius, R and mass, M_i is considered. The projectile displaces a vertical distance, x_i into an elastomer layer atop a rigid concrete half space. The design variables are taken to be the projectile impact velocity, V_0 and the properties of the elastomer layer, namely, the thickness, h_e and modulus, E_e.

For an incompressible (*i.e.* Poisson's ratio, $\nu = 0.5$) Neo-Hookean material, the principal stretches are related by $\lambda_1 \, \lambda_2 \, \lambda_3 = 1$. And, the strain energy per unit (undeformed) volume is given by:

$$U = \frac{E_e}{6} \left(\lambda_1^2 + \lambda_2^2 + \lambda_3^2 - 3 \right) \tag{1}$$

Note that a simpler strain energy potential is employed in the analytical model compared to the FE model of the spray-on elastomer coating. This is a reasonable approximation, given the simplified kinematics in the analytical model.

If the elastomer is assumed incompressible, then the principal Cauchy stresses, σ_i are related to U by [10]:

$$\sigma_i = -\alpha + \lambda_i \, \frac{\partial U}{\partial \lambda_i} \tag{2}$$

where α is an unknown scalar (interpreted as any applied hydrostatic pressure).

Since the deformation of the polymer layer under the indenter is complex, particularly in the vicinity of the corner (see Fig. 3), simplifying assumptions are required to progress with the analytical model. In the following, it is assumed that in all cases, the deformed material instantaneously under the indenter is in a state of uniaxial compression (interrogation of the stress contours in the numerical simulations reveal that this is a reasonable approximation). This implies that there is no effect of friction at the sliding interfaces, and no constraining effect of the polymer sheet in the vicinity of the indenter. Taking $\lambda_1 = \lambda = 1 - x_i/h_e$; $\lambda_2 = \lambda_3 = 1/\sqrt{\lambda}$; $\alpha = 0$, then the contact pressure under the projectile:

$$p = -\sigma_1 = -\lambda_i \frac{\partial U}{\partial \lambda_i} = -\frac{E_e}{6}\left(2\,\lambda - \frac{2}{\lambda^2}\right)\lambda \tag{3}$$

It therefore remains to relate the magnitude of λ to the projectile impact velocity.

This is achieved by equating the kinetic energy of the projectile to the maximum strain energy in the polymer (*i.e.* neglecting other sources of dissipation). To achieve this, the total strain energy in the polymer, $W(\lambda)$, is decomposed into two terms:

$$W(\lambda) = W_0(\lambda) + W_p(\lambda) \tag{4}$$

where $W_0(\lambda)$ is the strain energy in the material instantaneously under the projectile and $W_p(\lambda)$ is the strain energy in a perimeter zone in the vicinity of the projectile.

Considering a projectile of mass, M_i, impacting the elastomer with an initial velocity, V_0, applying conservation of energy for a maximum polymer stretch of, λ_{max}, gives:

$$\frac{M_i\,V_0^2}{2} = W(\lambda_{max}) \tag{5}$$

Throughout, to simplify the analysis, we assume that the presence of a perimeter strain energy does not alter the stress state under the indenter. (An alternative strategy, not pursued here, would be to account for the perimeter deformation through a constraining pressure, and hence the unknown constant, α in Eq. 2).

Examination of the FE results in Fig. 3 shows that the deformation in this perimeter zone is complex. Two models for the perimeter energy, $W_p(\lambda)$, are thus considered.

4.1. Model (i)

The simplest model is to assume that the perimeter energy is zero *i.e.* $W_p(\lambda) = 0$ in Eq. 4. The work done in deforming the polymer instantaneously under the projectile, as a

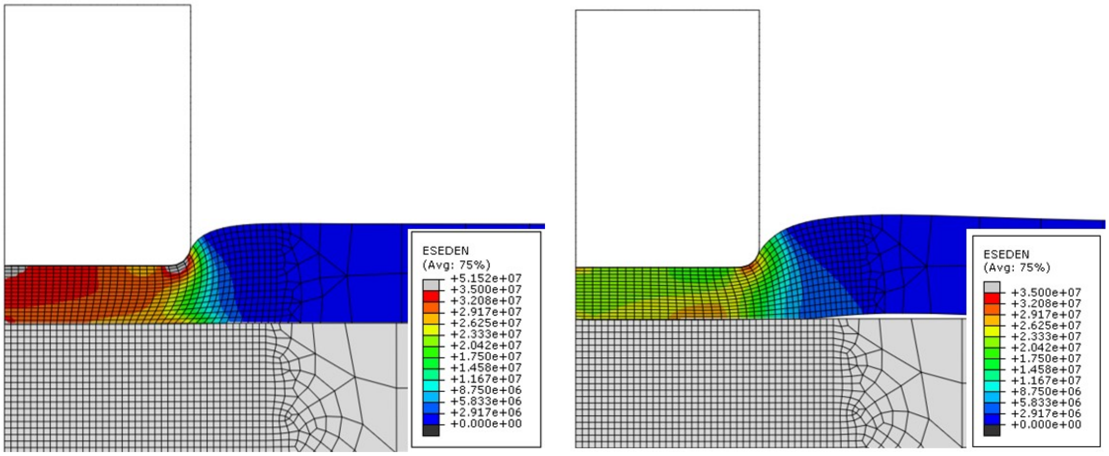

(a) Friction with coefficient, $\mu = 0.8$

(b) Frictionless

Figure 3: The elastic strain energy density (ESEDEN in ABAQUS notation) predicted by the FE model, at the instance of maximum projectile penetration depth, for a projectile impact velocity of $50\,\mathrm{m\,s^{-1}}$. Two variations on the FE model are considered: (a) frictional contact at the concrete/elastomer interface with a coefficient, $\mu = 0.8$ and (b) frictionless contact at the concrete/elastomer interface.

function of stretch, $W_0(\lambda)$, is therefore given by:

$$W(\lambda) = W_0(\lambda) = -\pi\, R^2\, h_e \int_1^{\lambda} p(\lambda)\, d\lambda = \frac{\pi\, R^2\, h_e\, E_e}{3}\Big(\frac{\lambda^3}{3} - \ln(\lambda) - \frac{1}{3}\Big) \tag{6}$$

Substituting into Eq. 5 will represent a lower bound on the energy absorbed by the coating.

4.2. Model (ii)

Alternatively, it can be assumed that the deformation in the perimeter zone matches that under the projectile (*i.e.* $\lambda_1 = \lambda$; $\lambda_2 = \lambda_3 = 1/\sqrt{\lambda}$). And so;

$$W(\lambda) = W_0(\lambda) + W_p(\lambda) = \pi\, R^2 h_e\, U(\lambda) = \frac{\pi\, R^2\, h_e\, E_e}{6}\,\Big(\lambda^2 + \frac{2}{\lambda} - 3\Big) \tag{7}$$

Substituting from Eq. 6 for $W_0(\lambda)$, the energy in the perimeter zone may be calculated:

$$W_p(\lambda) = \frac{\pi\, R^2\, h_e\, E_e}{3}\left(\frac{\lambda^2}{2} + \frac{1}{\lambda} - \frac{\lambda^3}{3} + \ln(\lambda) - \frac{7}{6}\right) \tag{8}$$

This would represent an upper bound on the perimeter energy. However, considering the FE results in Fig. 3, it is apparent that *Model (ii)* would significantly overpredict the deformation in the perimeter zone. This is particularly the case as x_i tends to h_e, as *Model (ii)* would give a perimeter energy (and perimeter radius) that tends to infinity.

4.3. Refined Model (ii)

Model (ii) can be refined by using a more general power law form of the strain energy in the perimeter zone:

$$W_p(\lambda) = \frac{\pi\, R^2\, h_e\, E_e}{3} \left(a\, (1-\lambda)^b \right) \tag{9}$$

Using a trial and error approach, the parameters, $a = 13/2$ and $b = 5$ in Eq. 9 are selected and match Eq. 8 reasonably well up to $\lambda \approx 0.2$, but tends to a finite perimeter energy for large projectile displacements (Fig. 4).

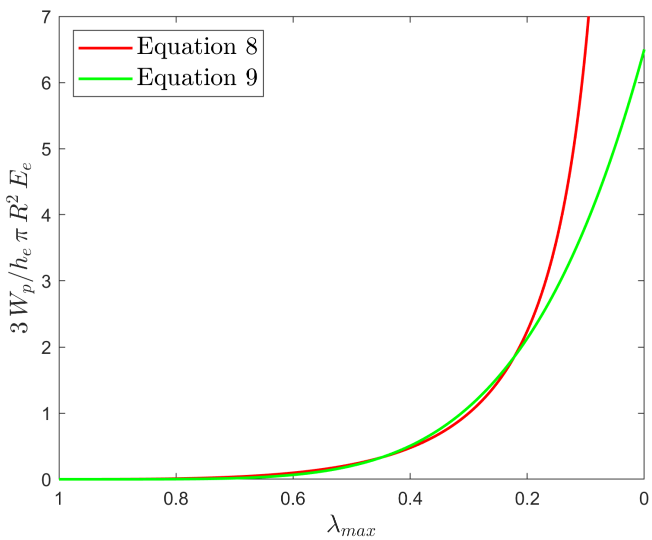

Figure 4: Analytical estimations of the strain energy in the perimeter zone according to Eqs 8 and 9, with $a = 13/2$ and $b = 5$.

This can be interpreted as a capped upper bound on the perimeter energy. Substituting Eqs 6 and 9 into Eq. 4, and then Eq. 5, yields the energy balance for impact from a projectile.

In the subsequent analysis, this refined version of *Model (ii)* is used.

4.4. Discussion: model applicability

It is noted that the proposed analytical model, and the underlying assumptions, make it applicable under the following conditions:

- The concrete target is large with respect to the indenter, and has a large modulus with respect to the polymer coating, so that it can be considered effectively a rigid half space.
- The impact velocities are sufficiently low with respect to the elastic wave speed in the polymer such that wave propagation effects can be neglected.
- The stiffness and strength of the projectile are high with respect to the polymer stiffness, so that it can be considered effectively rigid.
- The polymer layer thickness, h_e is sufficiently small with respect to the indenter radius so that the stress state under the indenter can be considered uniform through the polymer thickness.
- Viscous dissipation effects in the polymer are negligible. However, for realistic polymer coatings, and for the range of strain rates considered here, viscous effects have been shown to be present (for example, in [7] and [1]). Neglecting viscoelasticity underestimates the energy dissipated in the coating. Viscoelasticity may also change the way in which the coating deforms during dynamic indentation, which would also need to be accounted for in the analytical model, if significant. To account for viscous dissipation would however greatly complicate the analytical model, which is intended to provide a practical, first order indication of performance.

5. Critical impact velocities

Having derived relationships between the impact velocity, polymer deformation and contact pressure under the projectile, the next step is to determine critical values for failure of the target.

5.1. Concrete failure, $p = p_{crit}$

Hawkins [11] developed analytical expressions for the bearing strength of concrete members loaded through rigid plates. Since concrete sections can typically withstand a higher direct stress over a localised area compared to their compressive strength, the bearing strength is related to the compressive strength and the ratio of the load bearing area to the total area of the section. Hawkins' study considered the case of concentric loadings *i.e.* cubes loaded through a central square plate or cylinders loaded through a central circular plate which is assumed to be analogous to the present case of interest. A failure model, based upon observations from a large number of experimental tests is proposed. It assumes that for collapse, a limiting shearing stress develops on the surface of a failure cone directly under the indenter. The limiting stress on the failure plane can be described using the familiar Mohr-Coulomb (MC) failure criterion:

$$\tau = \tau_0 + \sigma \, \tan\psi \tag{10}$$

where τ is the shearing resistance on the failure plane, σ is the pressure normal to the failure plane, τ_0 is the shear strength at zero σ on the failure plane and ψ is the angle of internal friction. If the concrete compressive strength, σ_{cu} and tensile strength, σ_{to} are known; then ψ and τ_0 can be calculated from the geometry of the MC criterion. This leads to:

$$\frac{\sigma_{cu}}{\sigma_{to}} = \frac{1 + \sin\psi}{1 - \sin\psi} \tag{11}$$

$$\tau_0 = \frac{\sigma_{to}}{2}\left(\frac{1}{\cos\psi} + \tan\psi\right) \tag{12}$$

Hawkins' [11] failure model assumes that the concrete surrounding the loaded area is a stack of horizontal slices, each of which can deform without interference from the neighbouring slice. Inside these slices is the failure cone, which for collapse has developed a limiting stress on the surface of the cone, as defined previously. Assuming the radial pressures exerted by the punched cone splits the block, and based on equilibrium of the failure cone, the expression for the bearing strength, q is given by Eq. 13. This is equal to the concrete cylinder strength plus an additional component to represent the confining effect of the unloaded concrete surrounding the failure cone.

$$\frac{q}{\sigma_{ck}} = 1 + \frac{K}{\sqrt{\sigma_{ck}}}(\sqrt{A} - 1) \qquad for\, A < 40 \tag{13}$$

where σ_{ck} is the concrete cylinder strength which is $\approx 0.8\,\sigma_{cu}$. A is the ratio of the *effective* unloaded area to the loaded area. K is a constant which depends upon the characteristics of the concrete:

$$K = \frac{\sigma_{to}}{\sqrt{\sigma_{ck}}}\,\cot^2\alpha \tag{14}$$

where $\alpha = 45^\circ - \psi/2$.

Based on extensive comparisons with experimental tests, Hawkins recommends that the factor K can be taken as $50\,(\text{lb/in}^2)^{1/2}$ which equates to approximately $4.15\,(\text{MPa})^{1/2}$. For the geometry involved in this study, this gives a bearing strength estimate of 101 MPa.

However, calculating K for the concrete designed in [1], assuming $\sigma_{cu} = 47\,\text{MPa}$ and $\sigma_{to} = 5\,\text{MPa}$, then $K = 7.67\,(\text{MPa})^{1/2}$. Assuming an axisymmetric concrete domain of radius 50 mm, concentrically loaded by an indenter of radius 14.25 mm, this leads to a bearing strength estimate of 160 MPa which is in very close agreement with that measured in the quasi-static indentation experiments on uncoated concrete cubes, described in [1] and illustrated in Fig. 5.

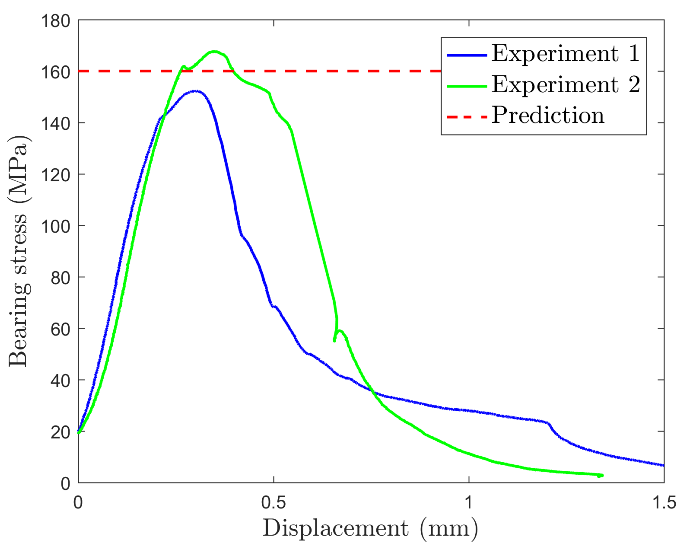

Figure 5: Bearing stress measured in the quasi-static indentation tests performed on two apparently identical concrete cubes in [1]. Also plotted is Hawkins' prediction of the bearing strength of the concrete specimen [11].

The analysis proceeds by assuming that the critical contact pressure to cause concrete failure, p_{crit}, is equivalent to Hawkins' estimate of the bearing strength, $q = 160\,\mathrm{MPa}$.

From Eq. 3, the stretch in the polymer is related to the contact pressure, p by:

$$\lambda^3 + \frac{3\,p\,\lambda}{E_e} - 1 = 0 \tag{15}$$

Solving Eq. 15 for λ and setting $p = p_{crit}$ yields an expression for λ as a function of p_{crit} and E_e. Substituting this for λ_{max} in Eq. 5 yields the energy balance at concrete failure. The *Model (i)* and *Model (ii)* predictions are derived by altering the assumptions about the elastic strain energy distribution in the polymer, discussed previously in Sections 4.1 and 4.3, respectively.

5.2. *Elastomer failure*

Of primary concern for coating design is to delay the point at which the concrete substrate fails. However, it is necessary to also estimate the conditions under which polymer failure might occur before concrete failure, as the response of the coated target is likely to change under those conditions. Setting $\lambda_{max} = \lambda_{crit}$ (*i.e.* the critical stretch to cause elastomer failure) in Eq. 5 yields the energy balance at elastomer failure. Once more, the *Model (i)* and *Model (ii)* assumptions are discussed in Sections 4.1 and 4.3, respectively.

The boundary between the *concrete failure* regime and the *elastomer failure* regime occurs when simultaneously, $p = p_{crit}$ and $\lambda_{max} = \lambda_{crit}$. Thus, from Eq. 3, the following relationship applies:

$$p_{crit} = \frac{E_e}{3}\left(\frac{1}{\lambda_{crit}} - \lambda_{crit}^2\right) \tag{16}$$

Setting $\lambda_{crit} = 0.1$ (*i.e.* $x_i = 0.9\,h_e$, indicative of the deformations at failure observed in experimental shear punch tests in [1, 7]), the model predicts that for $E_e < 0.3\,p_{crit}$, elastomer failure occurs before concrete failure (*i.e.* at a lower projectile impact speed, V_0). For $E_e > 0.3\,p_{crit}$, the model predicts a *concrete fails first* regime.

6. Design maps

A designer who wishes to protect a concrete structural element, of known strength, against impact from a projectile, of known mass and radius, can plot contours of critical projectile impact velocity using the equations set out in Sections 4 and 5. Thus, the designer can graphically visualise what combination of elastomer modulus and sprayed-on thickness would be required to protect against a particular impact velocity for their assumed projectile.

For a projectile of radius, $R = 14.25\,\mathrm{mm}$ and mass, $M_i = 0.1\,\mathrm{kg}$, and assuming $p_{crit} = 160\,\mathrm{MPa}$ and $\lambda_{crit} = 0.1$, the design maps illustrated in Fig. 6 are plotted. These maps plot contours of the critical projectile impact velocity for failure, V_{crit}. The solid lines indicate the model predictions for the critical impact velocity for concrete failure, which is of most interest to the designer. The predictions for elastomer failure are overlayed as dotted lines.

The boundary between the *elastomer fails first* and *concrete fails first* regimes occurs at a small strain elastomer modulus, $E_e = 0.3\,p_{crit} = 48\,\mathrm{MPa}$. Note that this regime change occurs at a value of E_e within a realistic range of elastomer moduli, representative of typical spray application elastomers. Plotting a marker, $\diamond$, at the location which corresponds to the elastomer coating tested in [1], it is noted that the coated concrete target is predicted to fall within the *concrete fails first* regime.

First, the *Model (i)* map in Fig. 6a is examined. Both the elastomer and concrete failure contours exhibit a similar shape. For very low polymer stiffnesses ($E_e < 5\,\mathrm{MPa}$), the critical impact velocity becomes very sensitive to the polymer modulus. Consequently, very thick coatings ($h_e > 10\,\mathrm{mm}$) are required to achieve a critical impact velocity in excess of $20\,\mathrm{m\,s^{-1}}$.

The sensitivity of V_{crit} at concrete failure to the polymer stiffness diminishes rapidly above the regime boundary at $E_e = 48\,\mathrm{MPa}$. This suggests that when designing within the *concrete fails first* regime, the critical design parameter is the polymer thickness, h_e. For the *Model (i)* case, in this regime, V_{crit} can reach values of about $60 - 70\,\mathrm{m\,s^{-1}}$ before the required coating thicknesses exceed $10\,\mathrm{mm}$.

For the high speed gas gun tests performed in [1], $E_e = 80\,\mathrm{MPa}$ and h_e varied between $5 - 6\,\mathrm{mm}$. Those tests predicted concrete failure for projectile impact velocities in the range $V_0 = 100 - 124\,\mathrm{m\,s^{-1}}$. The marker, $\diamond$, corresponding to these tests on Fig. 6a shows that concrete failure is predicted for $V_0 \approx 50\,\mathrm{m\,s^{-1}}$ which is considerably lower than that observed experimentally. Thus, the design map based on *Model (i)* appears rather conservative in terms of concrete failure predictions.

Next, the map based on *Model (ii)* is plotted in Fig. 6b. The regime boundary, at

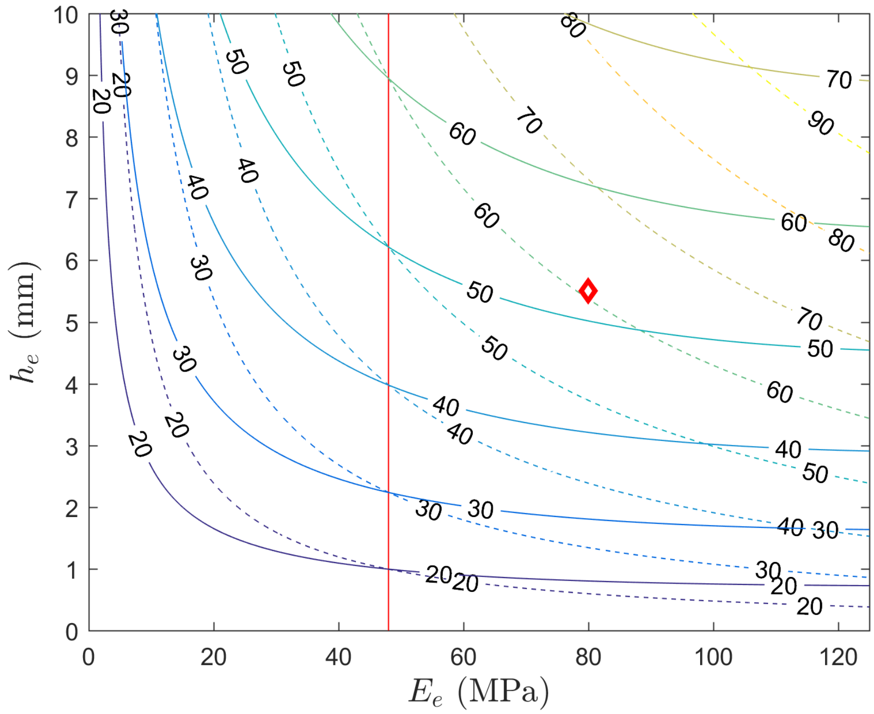

(a) *Model (i)*

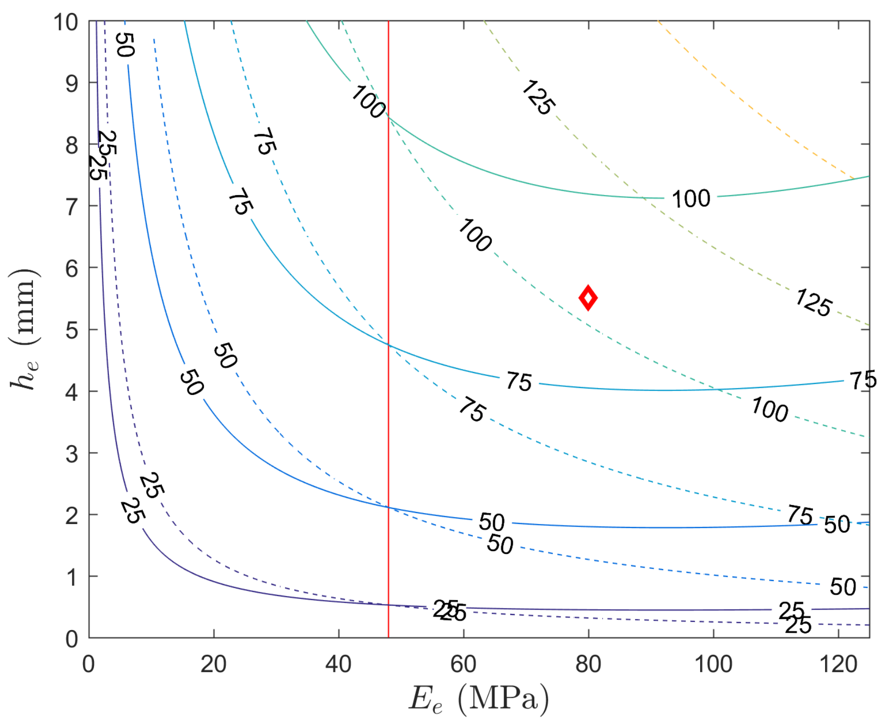

(b) *Model (ii)*

Figure 6: (a) *Model (i)* and (b) *Model (ii)* contours of V_{crit}. Solid lines indicate concrete failure and dotted lines indicate elastomer failure. To the left of the vertical red boundary, the model predicts elastomer failure before concrete failure; to the right, the model predicts concrete failure before elastomer failure. ◇ indicates the experimental test performed in [1] and referred to in the text.

$E_e = 48\,\mathrm{MPa}$ remains unchanged and both the concrete and elastomer failure contours are of a similar shape to those derived for *Model (i)*. Once more, in the *elastomer fails first* regime, very soft polymers require very large coating thicknesses ($h_e > 10\,\mathrm{mm}$) to sustain even very low impact velocities. Higher polymer stiffnesses are likely to be in the *concrete fails first* regime where the critical design parameter once more is the coating thickness. Upon closer examination of the concrete failure contours at higher impact speeds, for example, $V_{crit} = 75\,\mathrm{m\,s^{-1}}$ and $100\,\mathrm{m\,s^{-1}}$, there appears to be a particular value of the polymer modulus, E_e that minimises the coating thickness required. Taking $V_{crit} = 100\,\mathrm{m\,s^{-1}}$ for example, it appears that a polymer stiffness of around $E_e = 90\,\mathrm{MPa}$ is an optimum choice in terms of minimising the coating thickness required to prevent failure. It is noted however that there is only a weak sensitivity to polymer modulus in this regime.

The critical velocities predicted using *Model (ii)* differ significantly from those predicted by *Model (i)*. For a given E_e, h_e combination, the predicted V_{crit} is increased by almost a factor of two. The experimental gas gun tests (from [1]), represented by the marker, $\diamond$, on Fig. 6b measured concrete failure for projectile impact velocities in the range $V_0 = 100 - 124\,\mathrm{m\,s^{-1}}$. The *Model (ii)* analytical approach predicts failure for an impact velocity, $c.\,90\,\mathrm{m\,s^{-1}}$ which agrees well with the experiments. The discrepancy is likely due to the omission of viscous dissipation in the analytical model, as discussed in Section 4.4 which would serve to push the critical velocities for failure even higher. Nevertheless, the *Model (ii)* analysis appears to provide a good match to the experiments and in the following section, the validity of the models are assessed in more detail.

7. Validation cases

This section compares the analytical predictions of concrete failure with the results of the FE models and experiments (from Fig. 2). Figure 7 plots the *Model (i)* and *Model (ii)* analytical predictions for an elastomer coating with modulus, $E_e = 80\,\mathrm{MPa}$, subjected to impact from a projectile of mass, $M_i = 0.1\,\mathrm{kg}$ and radius, $R = 14.25\,\mathrm{mm}$. The model is compared with the experimental results, and the finite element analysis (the latter considering alternative friction conditions at the interfaces, as described subsequently).

Comparison with the experimental results is considered in Fig. 7a. The *Model (ii)* estimate provides the closest match with experimental results, though it provides a conservative prediction of the critical velocity to cause concrete failure. As discussed previously, viscous dissipation in the elastomer layer is omitted which, if included would serve to increase the predicted critical velocities. Furthermore, concrete strain rate dependence has been neglected which again, would serve to boost the concrete strength, elevating p_{crit} and thus the critical impact velocities for failure. Nevertheless, the analytical estimates, in particular the *Model (ii)* approach, give a good match to the experimental results.

Next, the analytical and FE predictions of concrete failure are compared. As described in Section 3, two variations of the FE model are considered: one with frictional contact at the elastomer/concrete interface and one with frictionless conditions at this interface. Quasi-static tests in [1] suggested best agreement was achieved with frictional contact whereas Fig. 2 shows that frictionless conditions bring the FE predictions more into line with the impact experiments. It can therefore be deduced that the rate of loading has an effect on the interface frictional conditions. For the FEA case with interface friction, in Fig. 7b, the true boundary between concrete failure/no failure occurs between the analytically derived *Model (i)* and *Model (ii)* predictions. Considering the FEA case without interface friction, in Fig. 7c (which matched the experiments well), the *Model (i)* prediction is overly conservative. Instead, the *Model (ii)* estimate provides a very close match to the failure boundary.

In summary, the analytical models perform very well in terms of predicting the boundary between concrete failure and no failure, when compared to experiments and FEA predictions. The *Model (i)* approach provides a conservative estimate of the critical projectile velocities for failure whereas the *Model (ii)* approach predicts the failure boundary with good accuracy. Further refinement of the analytical model to account for viscous dissipation effects in the polymer would likely bring the predictions even closer to the experimental and FE results.

8. Conclusions

Analytical models are developed in order to predict the onset of failure for an elastomer-coated concrete target subjected to blunt projectile impact. The model is validated against experimental observations and FEA predictions (based on work in [1]). Design maps are produced, predicting the critical projectile impact velocity for failure, V_{crit} based on two

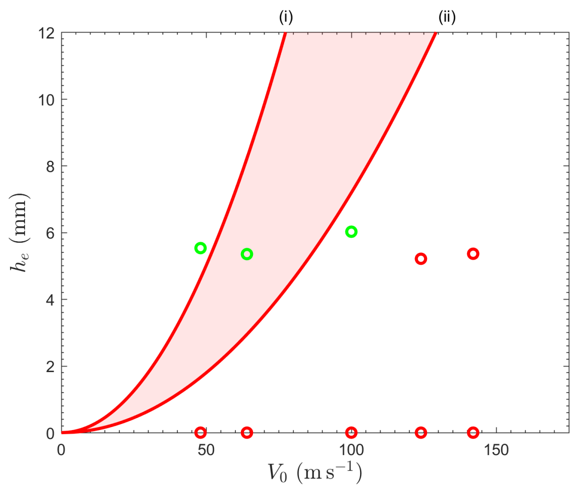

(a) Analytical predictions *vs* experiments

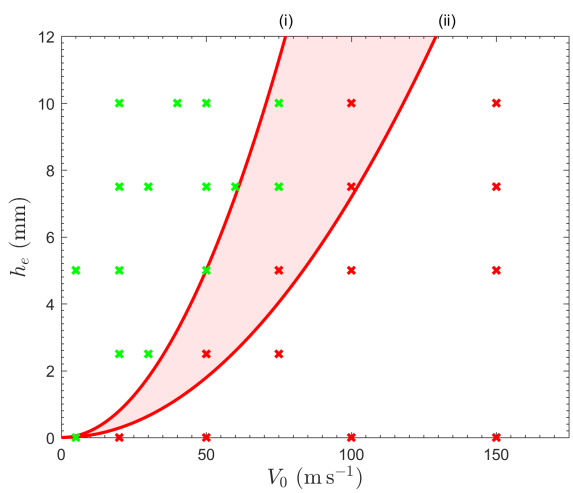

(b) Analytical predictions *vs* FE results (with friction)

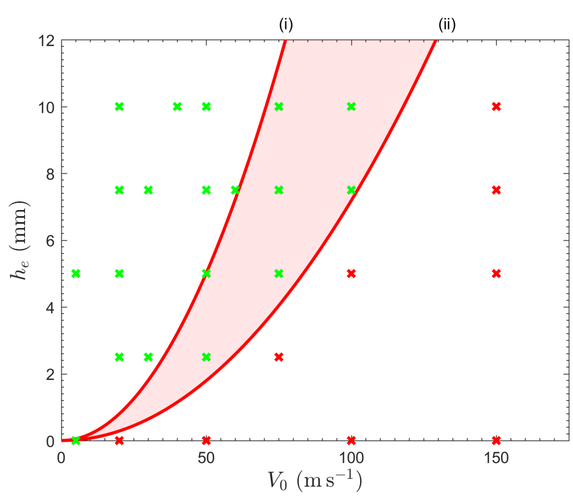

(c) Analytical predictions *vs* FE results (frictionless)

Figure 7: Comparing *Model (i)* and *Model (ii)* analytical predictions with (a) experimental observations, (b) FE results with frictional contact (coefficient, $\mu = 0.8$) at the elastomer/concrete interface and (c) FE results with frictionless contact at the elastomer/concrete interface. Legend: $\times$ represents FE predictions and $\circ$ represents experimental observations; green indicates intact concrete and red indicates damaged concrete.

design variables — the coating thickness, h_e and the elastomer modulus, E_e. The following conclusions are established:

- The analytical models are able to accurately predict the trends in critical projectile impact velocities as a function of polymer modulus and thickness, as shown by experiment and finite element analysis.

- The analytical predictions for critical projectile impact velocity are bounded by altering assumptions related to the distribution of elastic strain energy in the polymer.

- The *Model (i)* analytical estimates appear overly conservative, underestimating the critical failure velocities by approximately a factor of two when compared with experiments and FEA predictions.

- The *Model (ii)* analytical estimates are in closer agreement with experimental results and in particular, FEA predictions obtained by assuming frictionless contact at the elastomer/concrete interface.

- Over a realistic range of elastomer moduli, representative of typical spray application polymers, a regime change is predicted in the impact response of elastomer-coated concrete. It is predicted that the regime boundary depends only on E_e, and not h_e. For $E_e < 50\,\mathrm{MPa}$, it is predicted that the elastomer will fail first. For $E_e > 50\,\mathrm{MPa}$, the concrete is predicted to fail first.

- The analytical models also reveal key parameter sensitivities underlying protective coatings for concrete. In the polymer fails first regime, there is a much higher sensitivity to polymer modulus, E_e, compared to polymer thickness, h_e. In the concrete fails first regime, the critical velocity is most sensitive to the polymer thickness, and relatively insensitive to the modulus.

9. Acknowledgements

The authors are grateful to the George and Lillian Schiff Foundation of the University of Cambridge for financial support.

References

[1] Fallon, C., McShane, G. J., Impact mitigating capabilities of a spray-on elastomer coating applied to concrete, *International Journal of Impact Engineering*, Volume 128, Pages 72-85, June 2019

[2] Fallon, C., McShane, G. J., Impact damage protection mechanisms for elastomer-coated concrete, *submitted for publication*, 2020

[3] Knox, K. J., Hammons, M. I., Lewis, T. T. and Porter, J. R. (2000). Polymer Materials for Structural Retrofit. Air Force Research Laboratory, Air Expeditionary Forces Technology Division, Tyndall AFB, Florida

[4] Buchan, P. A. and Chen J. F., Blast resistance of FRP composites and polymer strengthened concrete and masonry structures – A state-of-the-art review, *Composites: Part B*, 38 (2007) 509-522

[5] Davidson, J. S., Porter, J. R., Dinan, R. J., Hammons, M. I., Connell, J. D. (2004). Explosive testing of polymer retrofit masonry walls. Journal of Performance of Constructed Facilities, 18(2), 100–106.

[6] Raman, S. N., Ngo, T., Mendis, P., Pham, T. (2012). Elastomeric Polymers for Retrofitting of Reinforced Concrete Structures against the Explosive Effects of Blast. Advances in Materials Science and Engineering, 2012, 1–8.

[7] Fallon, C., McShane, G. J., Fluid-structure interactions for the air blast loading of elastomer-coated concrete, *International Journal of Solids and Structures*, Volume 168, Pages 138-152, August 2019

[8] Fallon, C., McShane, G. J., Modelling the response regimes of elastomer-coated concrete subjected to blast pressure loading, *submitted for publication*, 2020

[9] Mauchien T.K., *A fracture mechanics approach to accelerated life testing for cathodic delamination at polymer/metal interfaces*, Master of Science in Engineering thesis, University of Texas at Austin, May 2013

[10] Holzapfel, G. A., *Nonlinear Solid Mechanics: A Continuum Approach for Engineering*, Chichester, Wiley, 2000

[11] Hawkins, N. M., The bearing strength of concrete loaded through rigid plates, *Magazine of concrete research*, 20(62):31-40, 1968